

Optomechanical deformation and strain in elastic dielectrics

M. Sonnleitner^{1,2}, M. Ritsch-Martel² and H. Ritsch¹

¹ Institute for Theoretical Physics, University of Innsbruck, Technikerstraße 25, A-6020 Innsbruck, Austria

² Division for Biomedical Physics, Innsbruck Medical University, Müllerstraße 44, A-6020 Innsbruck, Austria

E-mail: Matthias.Sonnleitner@uibk.ac.at

Abstract. Light forces induced by scattering and absorption in elastic dielectrics lead to local density modulations and deformations. These perturbations in turn modify light propagation in the medium and generate an intricate nonlinear response. We generalise an analytic approach where light propagation in one-dimensional media of inhomogeneous density is modelled as a result of multiple scattering between polarizable slices. Using the Maxwell stress tensor formalism we compute the local optical forces and iteratively approach self-consistent density distributions where the elastic back-action balances gradient- and scattering forces. For an optically trapped dielectric we derive the nonlinear dependence of trap position, stiffness and total deformation on the object's size and field configuration. Generally trapping is enhanced by deformation, which exhibits a periodic change between stretching and compression. This strongly deviates from qualitative expectations based on the change of photon momentum of light crossing the surface of a dielectric.

1. Introduction

As light carries momentum besides energy, its propagation through a polarizable medium is accompanied by forces. Although the momentum of a single light quantum is very small, laser light can generate appreciable forces on the microscopic scale. Optical forces are nowadays routinely used to manipulate and trap particles ranging from single atoms and molecules [1, 2, 3] to plastic beads, biological cells or microbes up to the size of tens of micrometres [4, 5, 6]. The mechanical motion of even larger objects such as silica microdisks or suspended mirrors has been damped and cooled by light forces [7, 8]. While most of the existing work targets the overall effect on the centre of mass of the particles, it has been shown by us as well as by other groups that these forces do not act homogeneously but exhibit distinct patterns within the medium [9, 10, 11]. For any elastic medium this leads to local compression or stretching. Of course the modified density also changes the local refractive index and light propagation, which again alters the forces as displayed schematically in figure 1. The resulting coupled complex evolution thus obviously requires self-consistent models and solutions. In addition, as the light

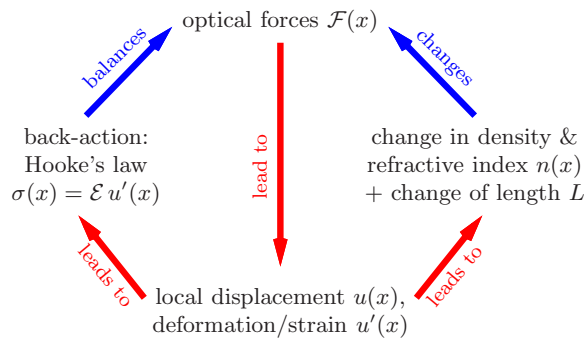


Figure 1. Schematic illustration of the interaction between optical forces and local deformations within elastic media.

mediated interaction is inherently long range, even a small but periodic variation of the refractive index can have a very large overall collective effect coupling distant areas over a large volume.

This work is organised as follows: In section 2 we first present the basic scattering approach to treat the light propagation in an inhomogeneous refractive medium and use a previously developed formalism based on the free space Maxwell stress tensor to calculate the corresponding local force distribution (section 3). This method is then used in section 4 to develop an iterative scheme to calculate the steady state density and field distribution as a function of geometry and field intensity. In section 5 we discuss essential physical consequences predicted by our model at the hand of numerical examples. Finally these results are compared to common calculations of the total deformation at hand of the change of photon momentum at an interface between to dielectrics, in section 6.

2. Multiple scattering model of light propagation in inhomogeneous media

The effective light propagation in a medium can be seen as the result of multiple individual scattering processes, which in general requires intricate numerical treatments, if one cannot make use of material symmetries. Here we restrict ourselves to the simple but still nontrivial case of two incoming counterpropagating plane waves in a transversely homogeneous and linearly polarizable medium. In this limit only forward and backward scattering add up phase coherently, while all amplitudes for transverse scattering average out. From the viewpoint of the forward and backward propagation directions, transverse scattering thus can just be added to an effective absorption rate in the medium. This is certainly not perfectly fulfilled in an actual setup, but still can be expected to give the correct qualitative behaviour, as long as the transverse extensions are much larger than the wavelength of the light. A more realistic treatment, e. g. in terms of Gaussian transverse beams, is possible, but greatly complicates the model and would obscure many interesting physical phenomena found in this simple approach.

Restricting the dynamics to the forward and backward scattering amplitudes along the propagation directions gives a simple and tractable model for our medium via a one dimensional array of N thin slices at positions x_1, \dots, x_N . Here the spatial behaviour of the electric field $\mathbf{E}(x, t) = \text{Re}[E(x) \exp(-i\omega t)]\mathbf{e}_y$ is determined by a 1D Helmholtz equation [12, 13, 11]

$$(\partial_x^2 + k^2)E(x) = -2k\zeta E(x) \sum_{j=1}^N \delta(x - x_j). \quad (1)$$

The field-induced polarisation density at each slice then is $P(x) = \alpha\eta_A E(x) \sum_{j=1}^N \delta(x - x_j)$, where we introduced the dimensionless coupling parameter $\zeta = k\eta_A\alpha/(2\varepsilon_0)$ proportional to the atomic polarizability α and the areal particle density η_A within the slice. ε_0 is the vacuum permittivity and $k = \omega/c$ the wave number of the optical field. Note that we assumed here that the dipoles in each slice can simply be added up coherently for scattering along the propagation direction. As illustrated in figure 2, the equation above is satisfied by interconnected plane wave solutions [12], here denoted as

$$E_j(x) := C_j e^{ik(x-x_j)} + D_j e^{-ik(x-x_j)} = A_{j+1} e^{ik(x-x_{j+1})} + B_{j+1} e^{-ik(x-x_{j+1})}, \quad (2)$$

for $x_j < x < x_{j+1}$. The amplitudes left and right of a material slice (beam splitter) at position x_j are connected via

$$\begin{pmatrix} C_j \\ D_j \end{pmatrix} = \begin{pmatrix} 1 + i\zeta & i\zeta \\ -i\zeta & 1 - i\zeta \end{pmatrix} \begin{pmatrix} A_j \\ B_j \end{pmatrix} =: M_{\text{BS}} \begin{pmatrix} A_j \\ B_j \end{pmatrix}. \quad (3)$$

The amplitudes (A_j, B_j) and (C_{j-1}, D_{j-1}) are coupled by a simple propagation matrix, i. e. $(A_j, B_j)^T = P_{d_j} (C_{j-1}, D_{j-1})^T$ with $P_{d_j} := \text{diag}(\exp(ikd_j), \exp(-ikd_j))$, with the distance $d_j := x_{j+1} - x_j$, $j = 1, \dots, N - 1$.

Therefore, the amplitudes to the left of the $(j + 1)^{\text{th}}$ slice are obtained by a simple multiplication of the previous transfer matrices,

$$\begin{pmatrix} A_{j+1} \\ B_{j+1} \end{pmatrix} = P_{d_j} M_{\text{BS}} \cdots P_{d_2} M_{\text{BS}} P_{d_1} M_{\text{BS}} \begin{pmatrix} A_1 \\ B_1 \end{pmatrix}. \quad (4)$$

The amplitudes A_1 and D_N are determined by the amplitudes and phases of waves coming in from the left (i. e. $-\infty$) and from the right ($+\infty$), respectively, and constitute boundary conditions on the solutions for the Helmholtz equation (1). B_1 and C_N are obtained by computing the total reflection and transmission amplitudes via

$$\frac{1}{t} \begin{pmatrix} t^2 - r_l r_r & r_r \\ -r_l & 1 \end{pmatrix} = M_{\text{BS}} P_{d_{N-1}} M_{\text{BS}} \cdots P_{d_2} M_{\text{BS}} P_{d_1} M_{\text{BS}}, \quad (5)$$

$$B_1 = r_l A_1 + t D_N \quad \text{and} \quad C_N = t A_1 + r_r D_N.$$

Note that the reflection coefficients for left or right incidence on an inhomogeneous setup usually do not coincide, i. e. $r_l \neq r_r$, but the transmission amplitude t is independent of the direction of propagation. More details on the properties of these generalised transfer matrices are given in Appendix A.

For equally spaced, thin polarizable slices we set $x_j = (j - 1)d_0$, such that $x_0 = 0$ and $x_N = (N - 1)d_0 =: L$ and (4) simplifies to $(A_{j+1}, B_{j+1})^T = T_{\text{h}}^j (A_1, B_1)^T$, with

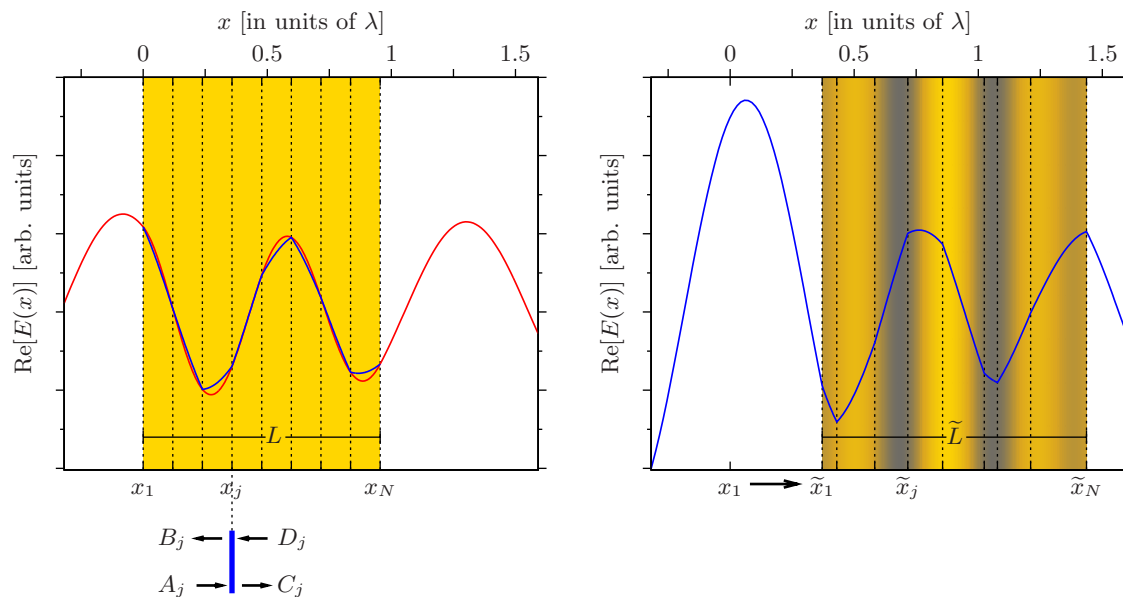


Figure 2. Schematic illustration of the displacement and deformation process $x \mapsto \tilde{x} = x + u(x)$. The initial medium (left figure) occupies the space $[0, L]$, the slices are marked with dotted lines separated by $d_0 = L/(N - 1)$. In this case, the field generated by multiple scattering by the beam splitters (blue curve, cf. (2)) reproduces the solution for a homogeneous medium with refractive index n (red curve), if the coupling is chosen as in (6). On the right hand side we see the displaced medium with irregularly spaced slices of the same coupling ζ and the resulting electric field. The background shading illustrates the change in the distances, i. e. the strain $u'(x) = -(\tilde{\rho}(x) - \rho)/\rho$, with dark colours indicating regions of higher density.

$T_h := P_{d_0} M_{BS}$. In an earlier work [11] we showed that choosing a uniform distance d_0 between the slices and setting the coupling parameter

$$\zeta = \frac{\cos(kd_0) - \cos(nkd_0)}{\sin(kd_0)} \quad (6)$$

leads to the same optical fields as found inside a medium with refractive index n . A sufficiently dense array of beam splitters with spacing $d_0 = L/(N - 1)$ is then in the limit $N \rightarrow \infty$ indistinguishable from a homogeneous medium of refractive index n and length L .

A decisive step in this work, which allows us to account for local material density variations, is the introduction of a local *displacement* variable $u(x)$

$$x_j \mapsto \tilde{x}_j = x_j + u(x_j), \quad j = 1, \dots, N. \quad (7)$$

As illustrated schematically in figure 2, such shifts alter the local fields as well as the total reflection and transmission properties of the object.

The distances between the slices then change as

$$\tilde{d}_j - d_0 = \tilde{x}_{j+1} - \tilde{x}_j - d_0 = u(x_{j+1}) - u(x_j) =: \Delta_j. \quad (8)$$

A continuous limit can be consistently defined via $u(x_j) \rightarrow u(x)$ for $x \in [0, L]$ to obtain

$$\lim_{N \rightarrow \infty} \frac{\Delta_j}{d_0} = \lim_{N \rightarrow \infty} \frac{u(x_j + d_0) - u(x_j)}{d_0} = u'(x). \quad (9)$$

In analogy with the theory of elastic deformations, we call u' *strain* or *deformation* [14, 15], and the relative change in the initially homogeneous local material density ρ simply reads

$$\frac{\tilde{\rho}(x) - \rho}{\rho} = -u'(x). \quad (10)$$

Let us here comment on the notation we will use for the rest of this work. As defined in the paragraph above (6), our coordinates are chosen such that the unperturbed medium occupies the region $[0, L]$. Introducing a displacement u then shifts the object to $[u(0), L + u(L)]$, with $L + u(L) - u(0) =: \tilde{L}$. But to ease notation, all the quantities such as the electric field strength E or force F shall remain defined with respect to the original position such that e.g. $E(0)$ [$E(L)$] always marks the field at the left [right] edge of the medium. The amplitudes at the boundaries then have to be adjusted with corresponding phases, cf. (22). This, however, is relevant for mathematical formulations only, physical discussions and figures are unaffected by this detail. In (7) we introduced a tilde to distinguish the shifted \tilde{x}_j from the original x_j . For most other quantities such as the fields or forces, we will omit this tedious notation. Only the changed length \tilde{L} , the inhomogeneous density $\tilde{\rho}$ (10) and refractive index \tilde{n} (19) still have to be distinguished from their original values L , ρ and n .

As mentioned before, defining the coupling ζ as in (6) ensures that the solutions of the wave equation (1) agree with the field inside a homogeneous dielectric at positions $x_j = (j-1)d_0$, if the fields are assumed to agree at x_1 . In the continuous limit $N \rightarrow \infty$, the latter requirement is always fulfilled [11]. Interestingly we still preserve this feature for a model with displaced slices, if we choose the following approach:

Let, as in (2), $E_j(x)$ denote the plain wave solution of the Helmholtz equation (1) and

$$E_{n_j}(x) = G_j e^{in_j k(x-x_j)} + H_j e^{-in_j k(x-x_j)} \quad \text{for } x_j < x < x_{j+1} \quad (11)$$

denote a field defined in the same region, but with a refractive index n_j . To obtain the desired equivalence between a stratified dielectric and a set of irregularly spaced slices, we assume for any given $j \in \{1, \dots, N-2\}$

$$\lim_{x \downarrow x_j} E_j(x) = \lim_{x \downarrow x_j} E_{n_j}(x) \quad (12)$$

and demand that with $E(\uparrow y) \equiv \lim_{x \uparrow y} E(x)$,

$$E_j(\uparrow x_{j+1}) = E_{j+1}(\downarrow x_{j+1}), \quad E'_j(\uparrow x_{j+1}) = E'_{j+1}(\downarrow x_{j+1}) + 2k\zeta E_{j+1}(\downarrow x_{j+1}), \quad (13)$$

$$E_{n_j}(\uparrow x_{j+1}) = E_{n_{j+1}}(\downarrow x_{j+1}), \quad E'_{n_j}(\uparrow x_{j+1}) = E'_{n_{j+1}}(\downarrow x_{j+1}), \quad (14)$$

$$E_j(\uparrow x_{j+1}) = E_{n_j}(\uparrow x_{j+1}), \quad E_{j+1}(\uparrow x_{j+2}) = E_{n_{j+1}}(\uparrow x_{j+2}). \quad (15)$$

The first line shows the conditions that E_j and E_{j+1} are solutions of the Helmholtz equation (1), cf. (3) or [12], the second line denotes Fresnel's equations for the transition between two dielectrics. In the third line, finally, we demand that the plane wave solutions of (1) agree with the fields inside the dielectrics at positions x_{j+1} and x_{j+2} .

This leads to the required, successive coupling between ζ , the distances $d_j = x_j - x_{j-1}$ and d_{j+1} , and some indices n_j, n_{j+1} .

Solving (13)-(15) under the assumption (12) and demanding solutions independent of the field amplitudes results in two conditions, for $j = 1, \dots, N - 1$

$$\frac{n_j \sin(kd_j)}{\sin(kn_j d_j)} = \frac{n_{j+1} \sin(kd_{j+1})}{\sin(kn_{j+1} d_{j+1})}, \quad (16)$$

$$\zeta = \frac{1}{2} \left[\frac{\cos(kd_j) - \cos(n_j k d_j)}{\sin(kd_j)} + \frac{\cos(kd_{j+1}) - \cos(n_{j+1} k d_{j+1})}{\sin(kd_{j+1})} \right]. \quad (17)$$

One can easily check that these conditions give the known relation (6) in the equidistant case where $d_j = d_{j+1} \equiv d_0$ and $n_j = n_{j+1} \equiv n$. Unfortunately, we were not able to find solutions with finite values of $d_j \neq d_{j+1}$ for both conditions. Inspired from (6) one may try

$$n_j = \frac{1}{d_j k} \arccos(\cos(d_j k) - \zeta \sin(d_j k)). \quad (18)$$

to find that this approach satisfies (17), but not (16). However, choosing ζ as in (6), writing $d_j = d_0(1 + \Delta_j/d_0)$, and taking the continuous limit $N \rightarrow \infty$ with $\Delta_j/d_0 \rightarrow u'(x)$ (9) alters (18) to

$$\tilde{n}(x) = \sqrt{\frac{n^2 + u'(x)}{1 + u'(x)}}, \quad (19)$$

satisfying both (16) and (17). With the given inhomogeneous refractive index we can compute the electric field inside a strained, one dimensional dielectric by solving

$$(\partial_x^2 + \tilde{n}^2(x)k^2)E(x) = 0 \quad (20)$$

numerically. A comparison with the field computed via the transfer matrix method described in (4) shows excellent agreement, for sufficiently large N .

Another way to approximate the optical field is to expand the transfer matrices in (4) for small local deformations Δ_j and then perform the continuous limit. This analytical approximation works sufficiently well for the typically small strain u' obtained in the scope of parameters used in this work. The lengthy results of this approach are presented in Appendix B, equation (B.6).

Inserting the relation between strain and density modifications (10) we finally obtain

$$\tilde{n}^2 = \frac{(n^2 + 1)\rho - \tilde{\rho}(x)}{2\rho - \tilde{\rho}(x)} \simeq n^2 + (n^2 - 1) \frac{\tilde{\rho}(x) - \rho}{\rho}, \quad (21)$$

where we assumed $(\tilde{\rho} - \rho)/\rho \ll 1$ for the final expansion.

2.1. Computing the reflection and transmission amplitudes

To find solutions for the fields inside the medium with refractive index distribution $\tilde{n}(x)$, one needs to specify initial values. As discussed for the discrete system in (5), the medium can be described in terms of a transfer matrix such that $B_0 = r_1 A_0 + t D_0$ and $C_L = t A_0 + r_r D_L$, if the electric fields outside the medium are given as $E(x) =$

$A_0 \exp(ikx) + B_0 \exp(-ikx)$ for $x \leq 0$ and $E(x) = C_L \exp(ik(x-L)) + D_L \exp(-ik(x-L))$ for $x \geq L$. The amplitudes A_0 and D_L are determined by the intensities $I_{l,r}$ and phases $\phi_{l,r}$ of the fields incident from the left and right and the displacement u , as

$$A_0 = \sqrt{\frac{2I_l}{\varepsilon_0 c}} e^{i\phi_l} e^{iku(0)} \quad \text{and} \quad D_L = \sqrt{\frac{2I_r}{\varepsilon_0 c}} e^{i\phi_r} e^{-ik(L+u(L))}. \quad (22)$$

Therefore, the initial conditions for solutions of (20) are $E(0) = A_0 + B_0$ and $E'(0) = ik(A_0 - B_0)$.

But obviously, the reflection and transmission coefficients r_l , r_r and t strongly depend on the refractive index $\tilde{n}(x)$. To calculate those one can either use some approximations, cf. Appendix B, equation (B.5), or solve the field equation (20) for specially chosen boundary values, e. g.

$$\begin{aligned} E^{[1]}(0) = iE^{[1]'}(0)/k = tD_L &\Rightarrow E^{[1]}(L) = D_L(r_r + 1), E^{[1]'}(L) = ikD_L(r_r - 1), \\ E^{[2]}(L) = -iE^{[2]'}(L)/k = tA_0 &\Rightarrow E^{[2]}(0) = A_0(1 + r_l), E^{[2]'}(0) = ikA_0(1 + r_l), \end{aligned} \quad (23)$$

allowing the easy computation of r_l , r_r and t .

It is easy to see that if $\tilde{n}(x)$ is symmetric, i. e. $\tilde{n}(x) = \tilde{n}(L - x)$, $x \in [0, L]$, then a beam entering from the left experiences the same medium as one from the right and hence $r_l = r_r$. Note that for the homogeneous case where $u' = 0$ and $\tilde{n} = n$, we recover the usual [16]

$$\begin{aligned} t_h &= \frac{2n}{2n \cos(nkL) - i(n^2 + 1) \sin(nkL)}, \\ r_h &= \frac{i(n^2 - 1) \sin(nkL)}{2n \cos(nkL) - i(n^2 + 1) \sin(nkL)}. \end{aligned} \quad (24)$$

3. Light forces in an inhomogeneous medium

In general, the total electromagnetic force on an object embedded in vacuum is given by [17]

$$F_\alpha = \oint_{\mathcal{A}} \sum_{\beta} T_{\alpha\beta} n_\beta dA, \quad (25)$$

where \mathcal{A} denotes the surface of the object, \mathbf{n} is the normal to \mathcal{A} and $T_{\alpha\beta}$ is the Maxwell stress tensor

$$T_{\alpha\beta} = \varepsilon_0 E_\alpha E_\beta + \frac{1}{\mu_0} B_\alpha B_\beta - \frac{1}{2} \delta_{\alpha,\beta} (\varepsilon_0 E^2 + \frac{1}{\mu_0} B^2). \quad (26)$$

Using two planes orthogonal to the direction of propagation (i. e. the x -axis) as integration surfaces and the plane wave fields defined in (2), the time-averaged optical force per area (pressure) on the j^{th} slice simply reads [18]

$$F_j = \frac{\varepsilon_0}{2} \left(|A_j|^2 + |B_j|^2 - |C_j|^2 - |D_j|^2 \right). \quad (27)$$

Following the beam splitter relation in (3) we rewrite $C_j = (1 + i\zeta)A_j + i\zeta B_j$ and $D_j = -i\zeta A_j + (1 - i\zeta)B_j$ to obtain

$$F_j = -\varepsilon_0 \left(|\zeta(A_j + B_j)|^2 - \text{Im}[\zeta(A_j + B_j)(A_j - B_j)^*] \right). \quad (28)$$

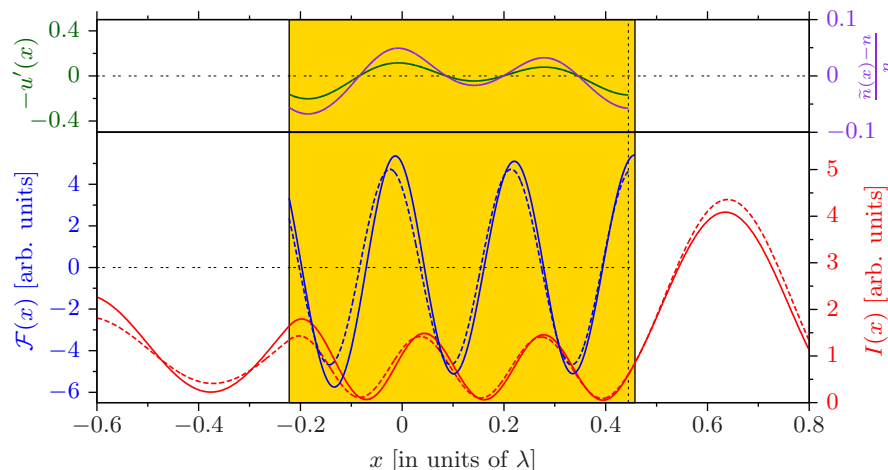


Figure 3. Illustration of the influence of a given strain u' (green) on the optical force density (blue) and the local intensity (red). The dotted lines show the homogeneous case $u' = 0$, the continuous lines represent the perturbations computed using the refractive index distribution $\tilde{n}(x)$ (purple). The reflection and transmission amplitudes here change from $r_h \simeq -0.29 - 0.29i$, $t_h \simeq -0.64 + 0.59i$ to $r_l \simeq -0.20 - 0.21i$, $r_r \simeq -0.15 - 0.24i$, $t \simeq -0.76 + 0.51i$. Please note that in this case the strain is not chosen such that it balances the optical forces as in (39).

Taking the naive limit $\lim_{N \rightarrow \infty} F_j$ would give a vanishing force per slice as $\lim_{N \rightarrow \infty} \zeta = 0$, cf. (6) with $d_0 = L/(N - 1)$. But assigning each slice to one N^{th} of the object's total length L we can define a force density $\mathcal{F}(x) := \lim_{N \rightarrow \infty} NF_j/L$ and use

$$\lim_{N \rightarrow \infty} \frac{N}{L} \zeta = k \frac{n^2 - 1}{2}. \quad (29)$$

Following the derivation of the inhomogeneous refractive index (19) we can replace $A_j + B_j = E_j(\uparrow x_{j+1}) = E_{n_j}(\uparrow x_{j+1}) \rightarrow E(x)$ (15) and in the continuous limit it is reasonable to set $A_j - B_j = -iE'_j(\uparrow x_{j+1})/k \rightarrow -iE'(x)/k$, if $E(x)$ is a solution of the wave equation (20). Hence we obtain the local optical force density

$$\mathcal{F}(x) = \frac{\varepsilon_0}{2} \text{Re}[(n^2 - 1)E(x)(E'(x))^*], \quad (30)$$

where we used the algebraic limit theorem for $\lim_{N \rightarrow \infty} N|\zeta|^2/L = 0$. Again, the results from the formula above are fully consistent with forces computed using a large but finite number of slices (4) and (27) as well as an analytical approximation presented in Appendix B, equation (B.9).

In figure 3 we compare the intensity and optical forces in a medium with homogeneous refractive index n to fields and forces obtained by solving (20) and (30), respectively, for a given strain u' .

3.1. Identification of radiation pressure and dipole force components inside a homogeneous dielectric

In the case of a medium with uniform refractive index n , i.e. with $u' \equiv 0$, the force density computed from (30) can be identified with established expressions for optical

forces on dielectric test particles. There, the time-averaged force on a dipole at position x_0 in the external field $E(x, t) = \text{Re}\{E(x) \exp(-i\omega t)\}$ with $E(x) = |E(x)| \exp(-i\varphi(x))$ reads [19]

$$F_L = \frac{1}{4} \partial_x |E(x_0)|^2 \text{Re} \alpha - \frac{1}{2} |E(x_0)|^2 \partial_x \varphi(x_0) \text{Im} \alpha, \quad (31)$$

where α is the polarizability of the dipole. The first term proportional to $\text{Re} \alpha$ is often referred to as *dipole* or *gradient force*, the (dissipative) term proportional to $\text{Im} \alpha$ is called *radiation pressure* or *scattering force* [19].

Inside a homogeneous dielectric we may write the spatial component of the electric field as $E(x) = G \exp(ink(x - x_0)) + H \exp(-ink(x - x_0))$, where the amplitudes G and H are chosen such that Fresnel's conditions at the boundary of the object are met. Using this field and rewriting (31) into a force density on particles with volume density η_V located at x_0 leads to

$$\mathcal{F}_L(x_0) = -\eta_V k \text{Im}\{GH^*\} \text{Re}\{\alpha n^*\} + \frac{k}{2} \eta_V (|G|^2 - |H|^2) \text{Im}\{\alpha n^*\}. \quad (32)$$

As the coupling parameter in (1) is defined as $\zeta = k\eta_A \alpha / (2\varepsilon_0)$, with η_A denoting the areal particle density in each of the N slices, we may write using (6) and (29)

$$\eta_V \alpha = \lim_{N \rightarrow \infty} \frac{N}{L} \eta_A \alpha = \lim_{N \rightarrow \infty} 2 \frac{N}{kL} \varepsilon_0 \zeta = \varepsilon_0 (n^2 - 1). \quad (33)$$

This relation also resembles the Lorentz-Lorenz relation for the case of a thin gas [16], where the individual dipoles do not directly interact with each other.

It can easily be checked that the force density in (32) together with the Lorentz-Lorenz relation (33) gives exactly the same result as the force computed from (30), if we insert the same field for a homogeneous dielectric. This demonstrates that our approach to calculate fields and forces from multiple scatterers is consistent with well known results derived from more general assumptions.

3.2. Integrated force and trap formation

To compute the total force on an extended dielectric in a standing wave we can use the same derivation as for the force on an infinitesimal slice in (27) and get

$$F_{\text{tot}} = \frac{\varepsilon_0}{2} \left(|A_0|^2 + |r_l A_0 + t D_L|^2 - |r_r D_L + t A_0|^2 - |D_L|^2 \right), \quad (34)$$

with A_0 and D_L denoting the amplitudes at the object's left and right boundaries, as given in (22). Defining the position of the centre of the object $x_0 = (u(0) + L + u(L))/2$, we can express the total force in terms of $\xi := x_0 + (\phi_l - \phi_r)/(2k)$

$$F_{\text{tot}}(\xi) = \frac{1}{c} (I_l s_l - I_r s_r + 2v \sqrt{I_l I_r} \cos(2k\xi + \psi)), \quad (35)$$

with $s_l = 1 + |r_l|^2 - |t|^2$, $s_r = 1 + |r_r|^2 - |t|^2$, $v = |r_l t^* - r_r^* t|$, $\psi = \arg(r_l t^* - r_r^* t)$.

If $4I_l I_r v^2 \geq (I_l s_l - I_r s_r)^2$, the force vanishes at every position $\xi_0 \in \Xi_+ \cup \Xi_-$ where

$$\begin{aligned} \Xi_+ &:= \left\{ \frac{m\pi}{k} + \hat{\xi}_0, m \in \mathbb{Z} \right\} & \text{and} & \quad \Xi_- := \left\{ \frac{m\pi - \psi}{k} - \hat{\xi}_0, m \in \mathbb{Z} \right\}, \\ \hat{\xi}_0 &:= \frac{1}{2k} \left(\arccos \left[\frac{I_r s_r - I_l s_l}{2v \sqrt{I_l I_r}} \right] - \psi \right). \end{aligned} \quad (36)$$

Using some trigonometric properties one can show that stable trapping positions are those defined in the set Ξ_+ . For $\xi_0 \in \Xi_-$ we find $F'_{\text{tot}}(\xi_0) > 0$ and hence Ξ_- is a set of unstable trapping position. Linearising the total force in (35) around stable trapping positions $\xi_0 \in \Xi_+$ leads to a trap stiffness of

$$\kappa = \frac{2k}{c} \sqrt{4I_1 I_r v^2 - (I_1 s_1 - I_r s_r)^2}. \quad (37)$$

Since the reflection and transmission coefficients strongly depend on the object's size, one finds that the parameter ψ can change its sign abruptly for certain values of L . This leads to sudden jumps between a low- and high-field-seeking behaviour for a trapped object [20, 21, 22, 11]. Figure 5 shows how trap position and trap stiffness is changed by the strain induced on the object by optical forces.

4. Self-consistent balancing of optical force and elastic back-action

In the previous chapters 2 and 3 we found expressions for the local fields and the local optical force densities in deformed, dielectric media. But depending on the given elastic properties, the strain will result in stress which typically tries to compensate the external volumetric forces.

In this chapter we will investigate the behaviour of a linear elastic, dielectric object subjected to the optical forces described by (30). More precisely, we will provide a framework to compute the equilibrium configuration between the optical forces and the elastic counter reaction in a self-consistent manner. In our computations we will assume only optical forces and neglect thermal or piezoelectric effects as well as surface tension.

Mechanical equilibrium between some general volume force density f and the resulting stress denoted by the tensor σ is given by Cauchy's equilibrium equation [15]

$$f_i + \sum_j \partial_j \sigma_{ij} = 0, \quad (38)$$

for i, j denoting the coordinates of the system. Since the model discussed here considers only one relevant dimension, this equilibrium equation simplifies to $f + \partial_x \sigma = 0$. The constitutive relation for a linear elastic, one dimensional object simply reads $\sigma = \mathcal{E}u'$, where \mathcal{E} is Young's modulus and u' is the local strain [15].

Hence we see that an equilibrium between the optical force density and the elastic strain requires

$$\mathcal{F}(x) + \mathcal{E}u''(x) = 0, \quad (39)$$

at every position $x \in [0, L]$, with \mathcal{F} being a solution of (30). Note that the electric field computed from (20) also depends on the amplitudes at the edges of the object and therefore also on the displacement u , cf. (22).

Solving (39) for an equilibrium requires boundary conditions on the displacement u and the strain u' which are determined by the given setup. The displacement is fixed by the assumed trapping mechanism, e. g. if the object is trapped by a standing wave, we have to fulfil $(u(0) + L + u(L))/2 \in \Xi_+$. But note that $\widehat{\xi}_0$ depends on the reflection and transmission coefficients and hence also on the deformation u' , cf. (36).

The strain has to be chosen such that the stress $\sigma = \mathcal{E}u'$ at each surface balances external *surface* forces [15]. Assuming for the moment an object subjected to volumetric optical forces only, we integrate the equilibrium equation (39) at obtain

$$0 = \int_0^L (\mathcal{F}(x) + \sigma'(x))dx = F_{\text{tot}} + \sigma(L) - \sigma(0). \quad (40)$$

For an object trapped by light fields, we get $F_{\text{tot}} = 0$ and $\sigma(0) = \sigma(L) = 0$, due to the lack of surface pressure. In chapter 5.2, however, we fix the slab by an external mechanism balancing the total optical force via surface interaction. Hence if the left boundary of the slab is retained at $x = 0$ (i. e. $u(0) = 0$), then $\sigma(L) = 0$ and $\sigma(0) = F_{\text{tot}}$.

To solve equation (39) numerically, we use an iterative approach where the equilibrium condition is rewritten in the form

$$\mathcal{F}(x)[u_i, u'_i] + \mathcal{E}u''_{i+1}(x) = 0, \quad (41)$$

with u_i and u'_i denoting the displacement and strain obtained by the i^{th} iteration step and $\mathcal{F}(x)[u_i, u'_i]$ is the force density computed using u_i and u'_i . The updated u'_{i+1} and u_{i+1} can then be obtained by simple numerical integration, with integration constants chosen in accordance to the boundary conditions of the used setup. With the updated optical force densities $\mathcal{F}(x)[u_{i+1}, u'_{i+1}]$ one can compute the next step of the iteration. An obvious choice for initial values is a homogeneously shifted distribution (i. e. a constant u_0) with a given starting length L and refractive index n .

This iterative scheme proved to be sufficiently exact but significantly faster compared to other methods of solving nonlinear equations, such as Newton's method. We also confirmed our computations with force densities obtained from the transfer matrix approach in (4) and the analytic approximation described in Appendix B, respectively.

5. Examples and physical interpretation

In our basic considerations above we always assumed the object to be exposed to two counterpropagating laser beams of the same, linear polarisation forming a standing wave. These results can easily be extended to describe situations with only one incident beam or with two counterpropagating beams of different polarisation. In the latter case, one has to calculate the intensities and forces separately for each polarisation direction.

In this section we will present four showcase examples to give insight into the large variety of possible results. The first two examples deal with the case where an object is trapped by two counterpropagating beams. The latter examples will treat the case where the object is illuminated by only one beam and externally fixed at one end. For each of the given examples one has to specify the boundary conditions for u and u' , as discussed in chapter 4.

For all considered setups we will see that the interaction between optical forces and elastic back-action strongly depends on the ratio between the initial length L and the wavelength of the deformation beam in the unperturbed medium, $\text{Re}[n]\lambda$. Concerning

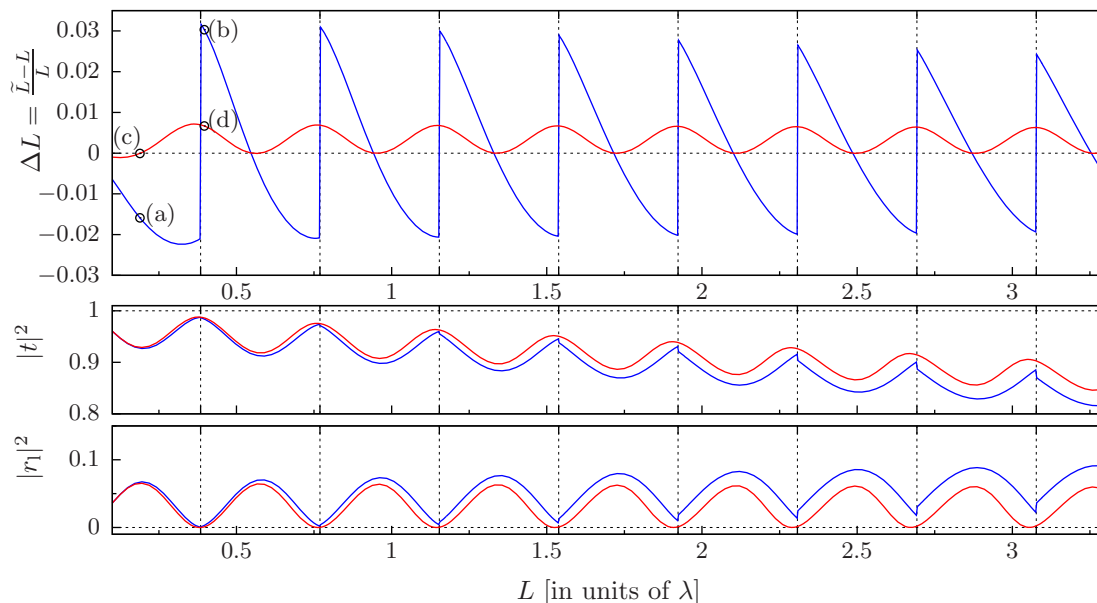


Figure 4. Relative length change, transmission $|t|^2$ and reflection $|r_1|^2$ for a dielectric slab trapped by two plane waves forming a standing wave (blue) or having orthogonal directions of polarisation (red lines). The incoming intensities and Young's modulus are related as $I_1 = I_r = 0.05\mathcal{E}c$, where c is the speed of light in vacuum; the refractive index is chosen as $n = 1.3 + 0.0025i$. The discontinuities in the standing-wave case stem from abrupt jumps in the stable trapping positions at $L = m\lambda/(2\text{Re}[n])$, $m \in \mathbb{N}$ (grid lines). The circles indicate the values used for the examples in figure 6 and 7.

the intensity and the elastic properties of the medium we find that all results grow linearly in $(I_1 + I_r)/(\mathcal{E}c)$, at least in the scope of parameters where a solution of the equilibrium equation (39) could be obtained within a reasonable error tolerance. That is why the local intensities, $I(x) = \varepsilon_0 c |E(x)|^2/2$, and force densities are given in units proportional to \mathcal{E} in the upcoming figures. Note that the numbers used in the simulations are unrealistic in order to exaggerate the effects, since an intensity of $I = 0.1\mathcal{E}c$ would imply $I \simeq 30\text{W}/\mu\text{m}^2$ for $\mathcal{E} \sim 1\text{MPa}$.

5.1. Example: Object trapped by two counterpropagating beams

As argued above, an object with initial length L subjected to optical forces will in general experience local deformations and an overall length change. Figure 4 shows the relative length change $\Delta L = (\tilde{L} - L)/L$ for different initial lengths L in the cases where an object is trapped in a standing wave (blue lines) or by two beams of orthogonal polarisation (red curves) and equal intensity. Obviously, both configurations are symmetric regarding an inversion of x at the centre of the object and therefore we find $r_1 = r_r$, as mentioned in section 2.1.

Surprisingly, in the standing wave case we observe abrupt switching from strong compressive to stretching behaviour around certain initial lengths. A comparison with chapter 3.2 and earlier discussions in [11] shows that these switches are concurrent with

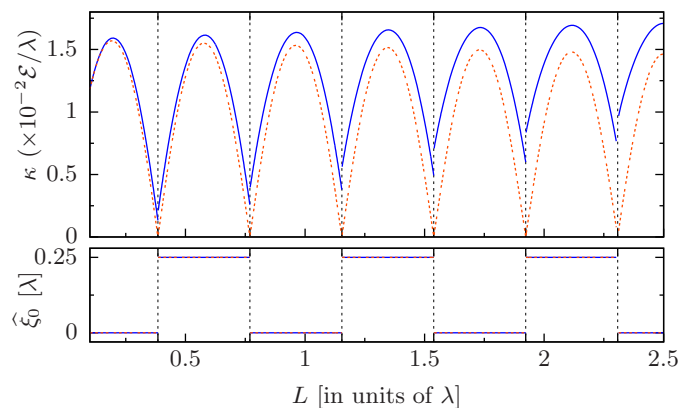


Figure 5. Trap stiffness κ (37) and stable trapping position $\hat{\xi}_0 \in \Xi_+$ (36) for an object trapped in a standing wave. The same parameters are used as in fig. 4, i. e. $I_1 = I_r = 0.05\mathcal{E}c$ and $n = 1.3 + 0.0025i$. A comparison of the blue curves denoting equilibrium solutions of (39) with the orange, dashed lines computed for the homogeneous objects shows that the deformation induced by optical forces significantly increases the total trapping strength. For the given case where $I_1 = I_r$, the trap positions remain unchanged.

jumps of the stable trapping position ξ_0 . Generally speaking, objects with small values of kL are trapped at local maxima of the intensity in the standing wave. But for larger objects, the term ψ in (36) abruptly changes its sign and the object seeks positions centred around intensity minima. As indicated by the dotted grid lines, these jumps occur at lengths of minimal reflection $|r_h|^2$ and maximal transmission $|t_h|^2$ (24), i. e. at $L = m\lambda/(2\text{Re}[n])$, $m \in \mathbb{N}$.

For larger objects we observe a slight decay of the maximal relative length change, which is found also for computations with $\text{Im}[n] = 0$ and thus is not caused by additional radiation pressure only. However, a glance at the reflectivity and transmission shows that the self consistent deformation prevents configurations with zero reflectivity which would usually result in maximum elongation or compression. For the given standing wave trap we generally observe that deformations computed with the steady state equation (39) tend to increase reflectivity and decrease transitivity compared to a homogeneous medium, for both $\text{Im}[n] = 0$ or $\text{Im}[n] \neq 0$.

In figure 5 we compare the trap stiffness κ from (37) and the trapping position $\hat{\xi}_0$ from (36) between unperturbed and self-consistently deformed objects. We find that the deformation significantly increases the trap stiffness, even if the total size of the object remains unchanged, cf. figure 4. An elastic object in a standing wave therefore assists in enforcing its own trap, just like a rabbit who starts to dig when captured in a pit. Note that for a compressible slab in a standing wave there is no critical length of zero trap stiffness, but deformation always leads to a stable trapping position.

Two examples for optical force densities and the associated deformation in the standing wave setup are shown in figure 6. There we see that the strain is negative (i. e. the material density is increased) at positions where the force density changes from

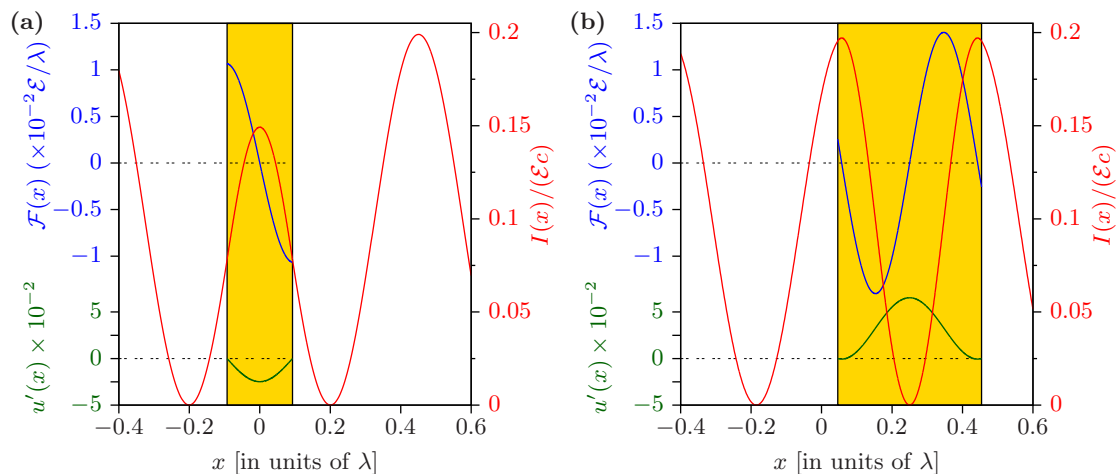


Figure 6. Dielectric objects trapped in a standing wave configuration with $I_1 = I_r = 0.05\mathcal{E}c$. The initial lengths are chosen as $L \simeq 0.19\lambda$ (a) and $L \simeq 0.4\lambda$ (b); $n = 1.3 + 0.0025i$. As mentioned in (10), positive strain $u'(x)$ (green curves) denotes larger distances between the particles and hence a reduction of material density. The density is increased at positions where the force density (blue lines) \mathcal{F} is zero and $\mathcal{F}' < 0$, i. e. where the light intensity (depicted red) has a maximum value. As indicated by the marks in figure 4 and verifiable from the signs of $u'(x)$, the object on the left gets squeezed whereas the right hand side example shows a stretched object.

positive values, denoting a force pushing to the right, to negative values associated with a force pushing to the left. One can clearly see the difference between the compressive situation (a) where the object is trapped at maximal intensity and situation (b), where the trapping occurs at minimal intensity and the object experiences a stretching force.

To trap a dielectric slab with two non-interfering plane waves of orthogonal polarisation, the intensities of said beams have to be equal, i. e. $I_1 = I_r$. In this case there are certain starting lengths $L \simeq (2m + 1)/(4\text{Re}[n])$, $m \in \mathbb{N}_0$, for which the intensities inside the unperturbed object add up to a constant value. Hence for these specific lengths the dominant gradient forces add up to zero and the object's length remains unchanged. Apart from that we find an expanding behaviour for $L > \lambda/(4\text{Re}[n])$, as can also be seen in the examples in figure 7.

In the case of non-interfering beams, figure 4 also shows that the reflectivity and transitivity is no longer periodic in the object's length L . For the reflectivity we find that the zeros are shifted from $L = m\lambda/(2\text{Re}[n])$, $m \in \mathbb{N}$, towards smaller lengths and no longer coincide with lengths of maximal elongation.

5.2. Example: Object fixed at the left boundary and illuminated by one beam.

Figure 8 shows the relative length change in the case where the left edge of a dielectric slab is fixed by some external mechanism. Here we observe a striking difference whether the object is illuminated from the left (blue) or right hand side (red curves). In the first case we find only stretching behaviour with minor oscillations of the relative length

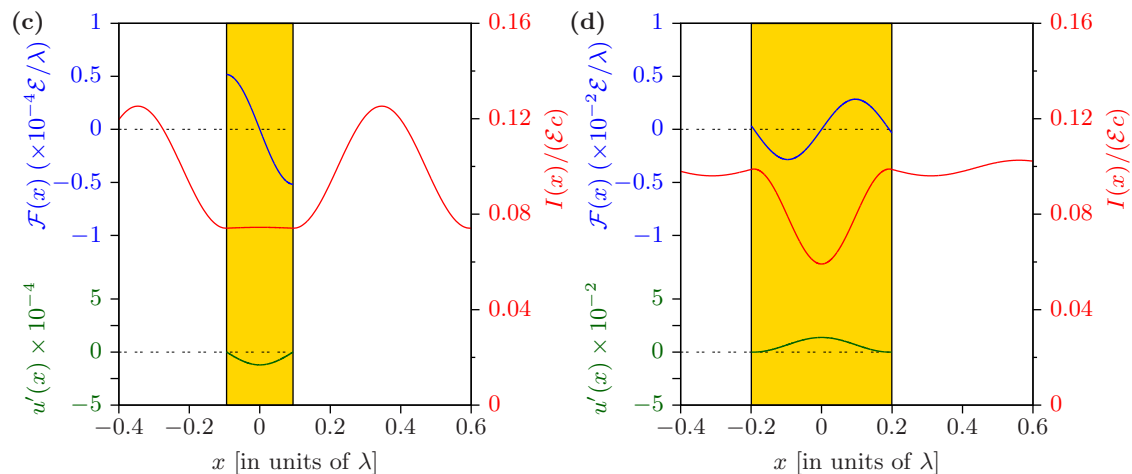


Figure 7. Dielectric objects trapped by two counterpropagating beams with orthogonal polarisation and $I_l = I_r = 0.05\mathcal{E}c$. As in figure 6, the initial lengths are $L \simeq 0.19\lambda$ (a) and $L \simeq 0.4\lambda$ (b); $n = 1.3 + 0.0025i$. As can be seen from figure 4, the length of the first example is chosen such that the intensities (red curves) inside the medium almost add up to a constant value. Hence the force densities (blue curves) and the self-consistent deformation (green lines) practically vanish (please note the changed scale on the axes). For the second example we obtain a stretching of $\Delta L \simeq 6.6 \times 10^{-3}$.

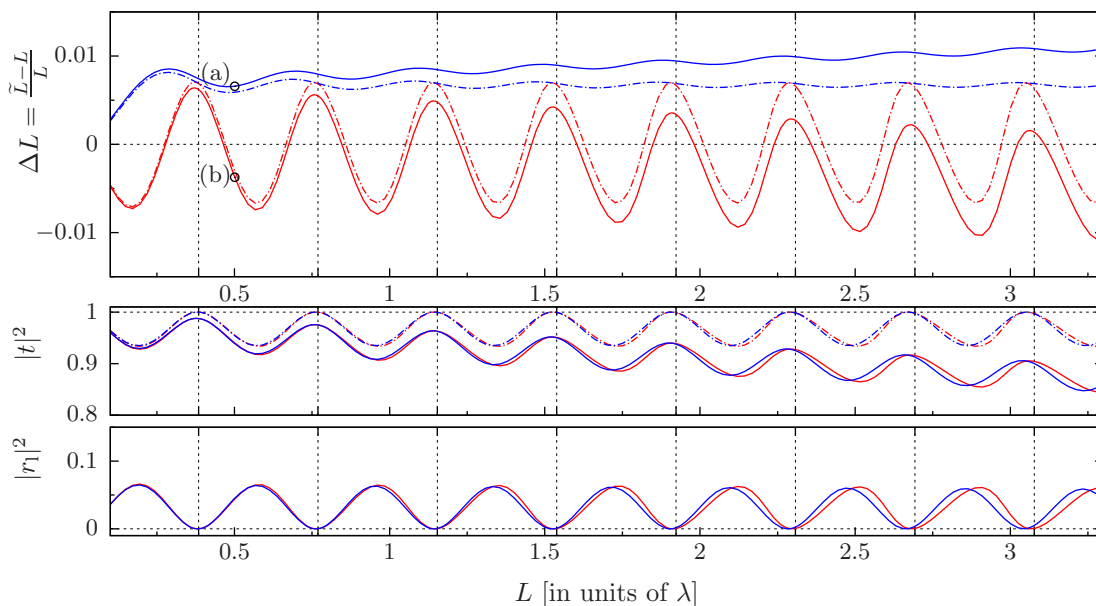


Figure 8. Relative length change, transmission $|t|^2$ and left reflection $|r_l|^2$ for a dielectric slab fixed at the left edge and illuminated by only one beam incident from the left (blue) or right (red) hand side, respectively. The initial refractive index is chosen as $n = 1.3 + 0.0025i$, the dash-dotted lines show the results for the non-absorptive case $n = 1.3$ (in the third plot for $|r_l|^2$ the additional lines were omitted to avoid ambiguity). The beams are of intensity $I_{l,r} = 0.1\mathcal{E}c$, the circles indicate the values used in figure 9. The grid lines mark the locations of the minima [maxima] of the reflectivity [transitivity] in the homogeneous case at $L = m\lambda/(2\text{Re}[n])$, $m \in \mathbb{N}$.

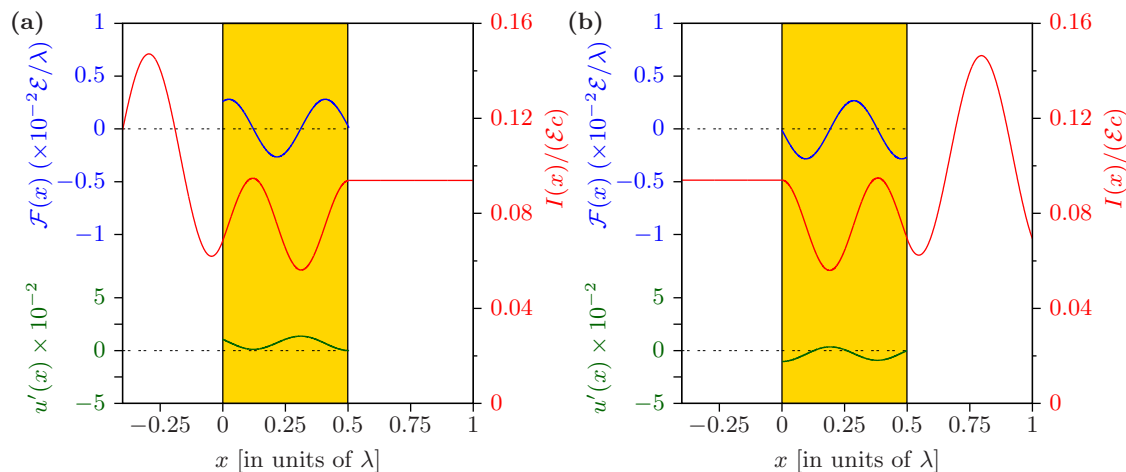


Figure 9. Two dielectric objects fixed at the left edge and illuminated from the left (a) or from the right hand side only (b), with $I_{l,r} = 0.1\mathcal{E}c$. As predicted from (42), the intensity (red) is locally maximal and the force densities (blue lines) are (almost) zero at the interface where light exits the slab. For left incidence we observe only positive (i. e. stretching) strain u' (green lines) whereas both elongating and compressive deformation is feasible for right illumination.

change ΔL . However, if the object is illuminated from the right hand side (i. e. the beam is incident on the free surface) we again find both compression and elongation, depending on the initial length L .

Furthermore we observe a stronger impact of absorption than for the previous case with two counterpropagating beams. Now we see that if $\text{Im}[n] \neq 0$, then ΔL increases (light incident from the left, radiation pressure pushing the object to the right) or decreases (light incident from the right) for larger initial lengths L . As we see from the dash-dotted lines, the length change continues to oscillate around a constant value also for large values of L , if $\text{Im}[n] = 0$.

For the reflectivity [transitivity], the self consistent strain again results in a shift of the minimal [maximal] values to the left of $L = m\lambda/(2\text{Re}[n])$, $m \in \mathbb{N}$. Note that for the given, asymmetric setup $r_1 \neq r_r$, but the difference in the total reflectivity $|r_1|^2 - |r_r|^2$ remains very low for the given parameters.

To explain the different results for left and right incident beams, we take a closer look at the interface where a single beam exits the slab, e. g. at hand of figure 9. Let us assume a beam entering from the left and $I_r = 0$. Then the intensity is not only constant on the right of the object, but Fresnel's formulae also tell us (for a homogeneous object)

$$\frac{d}{dx}I(L) = 0 \quad \text{and} \quad \frac{d^2}{dx^2}I(L) = k^2I(L)(1 - 2\text{Re}[n]^2 + 2\text{Im}[n]^2) \leq 0, \quad (42)$$

and hence the intensity has a local maximum at the edge where the beam exits the slab. For the usually dominant gradient force $\mathcal{F}_{\text{gr}}(x) \sim \frac{d}{dx}I(x)$ we thus find $\mathcal{F}_{\text{gr}}(L) = 0$ and $\mathcal{F}_{\text{gr}} > 0$ left of the surface. Considering the steady state equation (39) and omitting the scattering force shows that

$$\mathcal{F}(L) + \mathcal{E}u''(L) \simeq \mathcal{F}_{\text{gr}}(L) + \mathcal{E}u''(L) = 0 \quad (43)$$

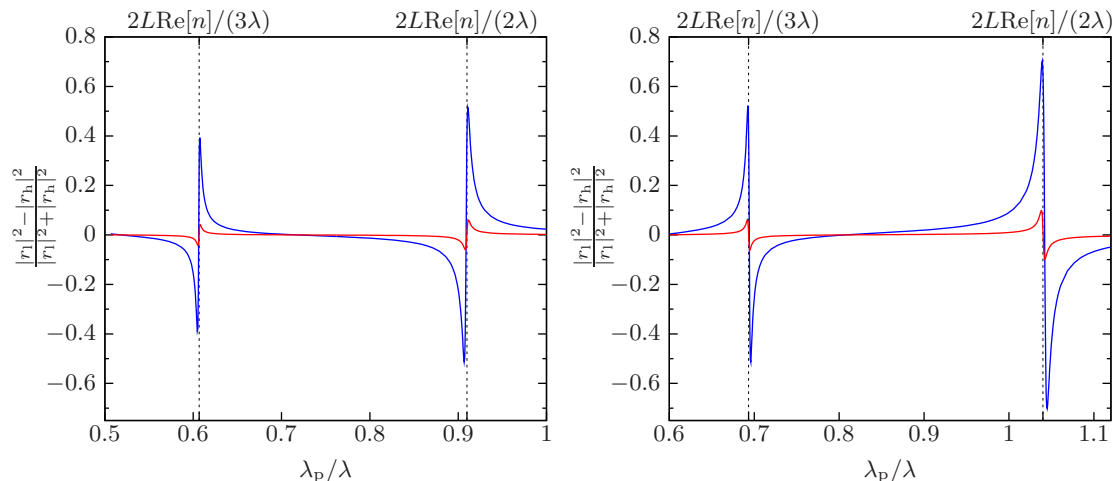


Figure 10. Relative change in the reflectivity of a strained object for different probe laser wavelengths λ_p , for slabs trapped in a standing wave pattern with $I_l = I_r = 0.0005\mathcal{E}c$ (red) and $I_l = I_r = 0.005\mathcal{E}c$ (blue curves), $n = 1.3 + 0.0025i$. In the left frame we used an initial length $L = 0.7\lambda$ and obtained compressive behaviour with $\Delta L \simeq -0.2 \times 10^{-3}$ (red) and $\Delta L \simeq -2.0 \times 10^{-3}$ (blue). The results on the right indicate stretching with $\Delta L \simeq 0.3 \times 10^{-3}$ (red) and $\Delta L \simeq 3.1 \times 10^{-3}$ (blue) for $L = 0.8\lambda$.

and hence the strain u' has a local minimum at the right edge $x = L$. If light enters only from the right hand side we find analogous behaviour for the left edge $x = 0$. Since minimal strain corresponds to a maximum in local material density (10), we conclude that the gradient force tends to accumulate material at the surface where a single light beam exits the object. A similar statement holds for the aforementioned case with two counterpropagating beams oscillating in orthogonal polarisations, but then one has to add up the forces generated by the two beams.

In total, the constraints on the strain as derived from (42), (43) and chapter 4 are found as

$$\text{left incidence only, } I_r = 0 : \quad u'(0) = \mathcal{F}_{\text{tot}}/\mathcal{E} \geq 0; \quad u'(L) = 0, \text{ is a minimum,} \quad (44)$$

$$\text{right incidence only, } I_l = 0 : \quad u'(0) = \mathcal{F}_{\text{tot}}/\mathcal{E} \leq 0, \text{ is a minimum;} \quad u'(L) = 0. \quad (45)$$

So if $I_l = 0$, the strain is fixed at a minimum with negative value on the left edge, at zero on the right edge, and oscillates proportional to the intensity in between. So in total we find both negative (compressive) and positive (expanding) deformation, depending on the length and refractive index of the object. For $I_r = 0$ we see a positive strain at the left edge and a minimum with $u'(L) = 0$ at the right boundary. Hence the deformations oscillate between zero and some positive value and always lead to a total stretching behaviour.

5.3. Identifying length changes by probing the reflectivity

As one can see from figures 4 and 8, the relative length change ΔL obtained for a given ratio of total intensity to Young's modulus can be imperceptibly small, especially if

the original length is not chosen in an optimal relation to the vacuum wavelength of the trapping beam, λ . But one possibility to detect minor stretching or squeezing for arbitrary initial lengths can be found in the use of a second, weaker laser probing the change in the reflectivity of the medium: Assuming a non-dispersive medium, a probe laser with a vacuum wavelength matching the Fabry-Pérot condition

$$\lambda_p \simeq \frac{2L\text{Re}n}{m}, \quad m \in \mathbb{N}, \quad (46)$$

will travel through a slab of length L without being reflected, i. e. $|r_h(\lambda_p)|^2 \simeq 0$. Turning on a powerful laser will deform the object and hence also change the reflectivity for the weak probe beam. Figure 10 shows the relative change of reflectivity

$$\delta R = \frac{|r_l|^2 - |r_h|^2}{|r_l|^2 + |r_h|^2} \quad (47)$$

between the unperturbed and the strained medium for different wavelengths of the probe laser beam. We can see that as λ_p crosses values defined in (46), δR changes from negative to positive values if the object is compressed (i. e. $\Delta L < 0$) and vice versa if $\Delta L > 0$.

6. Estimating the deformation by computing the photon momentum transfer on a surface

There are numerous experimental and theoretical works on the observed optical stretching of deformable objects, such as biological cells [23, 24], or light induced outward bending of liquid-gas surfaces [25, 26]. In the mentioned publications, the light-induced deformation is estimated by considering an effective photon momentum change at the transition from one medium to another. In this context, the optical forces emerge as surface forces, acting on the interface between two regions of different refractive index. Since the considered materials are incompressible, the refractive index in each region remains constant.

Let us try here a similar approach to estimate the deformation of an elastic object and put our results in context with these earlier works. But note that the very different physical properties of a linear elastic medium as compared to incompressible water, plane waves instead of Gaussian beams and a wave description instead of geometric optics, do not allow a straightforward comparison of the results.

Following the line of [23, 25, 24] one estimates the time averaged force per area on an interface separating two regions with different indices of refraction $n_1 \neq n_2 \in \mathbb{R}$ and fields $E(x) = A \exp(in_1 kx) + B \exp(-in_1 kx)$, $x \leq 0$, and $E(x) = C \exp(in_2 kx)$, $x > 0$, as

$$F_{1,2} = \frac{\Delta p}{\Delta t} = \frac{I_{\text{inc}}(p_1(1 + R) - p_2 T)}{\hbar k c}. \quad (48)$$

Here $I_{\text{inc}} = n_1 c \varepsilon_0 |A|^2 / 2$ is the total energy-flux density entering the system, $R = |B|^2 / |A|^2$ and $T = n_2 |C|^2 / (n_1 |A|^2)$ is the reflected and transmitted fraction the energy-flux and $p_i = \hbar k n_i$ describes the momentum of a single photon in a medium with

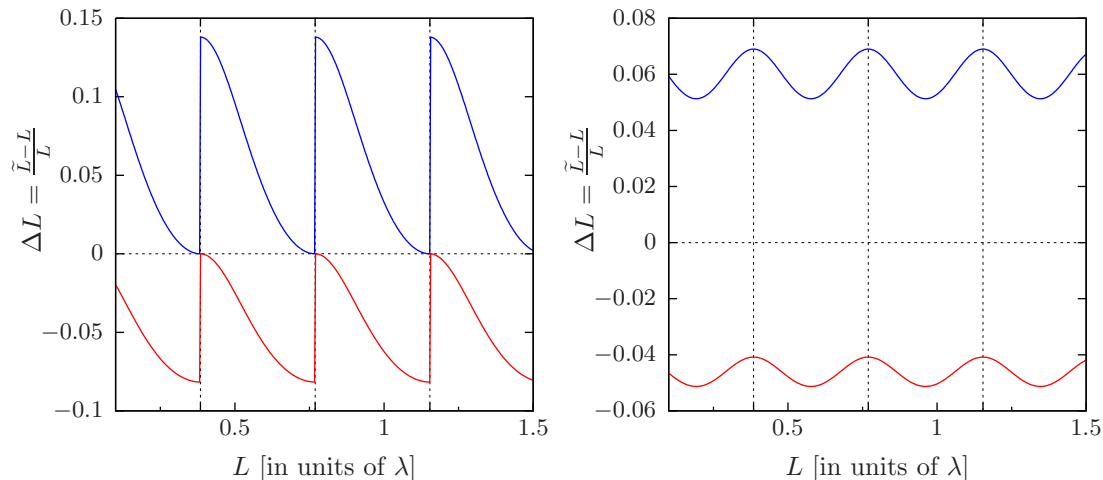


Figure 11. Expected deformation due to the change in photon momentum at the interfaces between vacuum and a homogeneous dielectric of refractive index $n = 1.3$, as obtained from (50). For the blue lines we used Minkowski's photon momentum $p = \hbar kn$, the red curves are computed using Abraham's $p = \hbar k/n$. The left figure shows the situation where a homogeneous object is trapped by a standing wave with $I_1 = I_r = 0.05\mathcal{E}c$. As in figure 4, the deformation changes abruptly, if the object switches from a low-field to a high-field seeking behaviour. The right hand figure depicts the relative length change for an object illuminated from only one side with $I_1 = 0.1\mathcal{E}c$, $I_r = 0$. In both situations we find that Minkowski's momentum only leads to stretching, whereas the naive adaption of Abraham's photon momentum would solely result in compression.

index n_i , $i = 1, 2$. As in [23, 24, 25] we here used Minkowski's version of the momentum of light in dielectric media. Out of curiosity about simple but puzzling arguments on stretching or compression of media in connection with the Abraham-Minkowski controversy [25, 27, 28] we also included results computed by naively inserting Abraham's result for the photon momentum, $p_i = \hbar k/n_i$, in figure 11. One must note, however, that Abraham's stress tensor would also require a material tensor component. A thorough calculation should always give the same results, independent of the used version of stress tensor [27, 28].

Neglecting internal reflections, the force on an extended object with index n_2 embedded in a medium n_1 and subjected to a single beam is estimated to give $F_{\text{tot}} = F_{1,2} + TF_{2,1}$. The deformation of such an object is then simply the difference in the two forces on the surfaces, reading $F_{\text{def}} = TF_{2,1} - F_{1,2}$. Assuming a linear elastic medium with Young's modulus \mathcal{E} , the relative length-change can be estimated by $\Delta L = F_{\text{def}}/\mathcal{E}$. For the values used in the previous examples $n_1 = 1$, $n_2 = 1.3$, $I_0 = 0.1\mathcal{E}c$, we obtain $\Delta L \simeq 0.059$ when using Minkowski's momentum and $\Delta L \simeq -0.046$ for Abraham. These deformations have about the same order of magnitude as our full self-consistent computations, depicted e. g. in figure 8, but do not depend on the length of the object.

Formally one can refine these calculations from (48) and include also light incident

from the right such that $E(x) = C \exp(in_2 kx) + D \exp(-in_2 kx)$, $x > 0$ to obtain

$$F_{1,2} = \frac{\varepsilon_0 n_1 p_1}{2\hbar k} (|A|^2 + |B|^2) - \frac{\varepsilon_0 n_2 p_2}{2\hbar k} (|C|^2 + |D|^2). \quad (49)$$

For $D = 0$ this reduces to (48) and for $n_1 = n_2 = 1$ and $p_1 = p_2 = \hbar k$ we recover the force derived previously with the Maxwell stress tensor (27). This allows to formulate a generic wave optics extension for the deformation estimated above in the scope of geometric optics, now including also size dependent reflection and transmission. The total deformation pressure on an object with length L and homogeneous refractive index $n \in \mathbb{R}$ surrounded by vacuum then reads

$$F_{\text{def}} = \frac{\varepsilon_0 n p_n}{\hbar k} (|G|^2 + |H|^2) - \frac{\varepsilon_0}{2} (|A|^2 + |B|^2 - |C|^2 - |D|^2) \quad (50)$$

where the amplitudes inside the medium are computed using Fresnel's relations $G = ((n+1)A + (n-1)B)/(2n)$, $H = ((n-1)A + (n+1)B)/(2n)$, the amplitudes outside are connected by the homogeneous reflection and transmission coefficients (24), $B = r_h A + t_h D$, $C = t_h A + r_h D$, and the incoming A and D are given in (22). As expected, a similar calculation for the total force F_{tot} gives the same result as we obtained previously in (34).

The resulting relative length change $\Delta L = F_{\text{def}}/\mathcal{E}$ is presented in figure 11. There we find that the estimations using optical surface forces even qualitatively differ from the results we obtained with the present description using the full, volumetric optical forces, cf. figures 4 or 8, even if the force on the surface is adapted to include interference due to internal reflections.

An intuitive example is the object of length $L = \lambda/(2n)$ where $r_h = 0$ and $t_h = 1$. In a standing wave trap with $I_l = I_r$ this object is then trapped at $\xi_0 = x_0 + (\phi_l - \phi_r)/(2k) = 0$, cf. chapter 3.2 or figure 5. Using Minkowski's $p_n = \hbar k n$ we then find that the force due to photon momentum transfer vanishes at each surface and hence $\Delta L = 0$ in figure 11. But from the examples in figure 6 we deduce that the intensity at the *surface* is zero, yet the object will contract due to the intensity maximum at its central position. This shows that describing optical deformation forces on a dielectric by a change in the photon momentum at its surface obscures many effects which are apparent in a full treatment involving volumetric forces.

7. Conclusions

Using an implicit calculation of optical fields and forces allows to self-consistently determine the stationary local deformations of an elastic object, where the local stress balances the local light forces by elastic back action. These solutions show a surprisingly variable and nonlinear dependence on the chosen parameters. Generally we see a length and illumination dependent, spatially quasiperiodic strain pattern, which can lead to length stretching as well as compression. As expected, standing wave configurations yield the strongest forces and effective length changes with a clear resonant structure for special ratios of initial object length L and trap beam wavelength λ . In the standing

wave setup, variations in the trap wavelength λ lead to discrete jumps of the stable trapping positions. At $L = m\lambda/(2\text{Re}[n])$, $m \in \mathbb{N}$, the particle switches from a position centred around an intensity maximum to one around a field node, which is associated with changes from compression to elongation of the object. Interestingly, in particular close to these instability points, this generally leads to an increase in trap stiffness. We expect that this indicates possible bistability between high and low field seeking behaviour for certain lengths very close $L = m\lambda/(2\text{Re}[n])$.

Although the calculations presented here were performed in the scope of elastic media, we believe that the model can be extended to deformable but incompressible media like water or even dilute gases. Here in particular stability thresholds for the homogeneous solutions should prove physically very interesting, as they could lead to stationary flows, periodic density oscillations or light induced density pattern formation and particle ordering in a gas.

Here we limited our considerations to the case, where a steady state solution can be found. As for other nonlinear dynamical effects [13], there are of course regions in parameter space, where no stationary solutions exist and we find self sustained oscillations or even disintegration of the material. Indications of this behaviour appear e.g. in a non converging iteration procedure. At this point we leave this to future work.

Acknowledgments

We thankfully acknowledge support via ERC Advanced Grant (catchIT, 247024) and the Austrian Science fund FWF grant S4013.

Appendix A. General features of transfer matrices

In equation (3) we already used the concept of a transfer matrix to couple the plane wave amplitudes left and right of a beam splitter. Let us generally define the set of transfer matrices as

$$\mathcal{T} := \left\{ T \in \mathbb{C}^{2 \times 2} \mid \exists r_1, r_2, t \in \mathbb{C} : T = \frac{1}{t} \begin{pmatrix} t^2 - r_1 r_2 & r_2 \\ -r_1 & 1 \end{pmatrix} \equiv T(r_1, r_2, t) \right\}. \quad (\text{A.1})$$

One can easily show that $T_1 \cdot T_2 \in \mathcal{T}$ for all $T_1, T_2 \in \mathcal{T}$ and \cdot here denoting the usually omitted matrix multiplication. Since also

$$[T(r_1, r_2, t)]^{-1} = \frac{1}{t} \begin{pmatrix} 1 & r_1 \\ -r_2 & t^2 - r_1 r_2 \end{pmatrix} \in \mathcal{T} \quad (\text{A.2})$$

we conclude that (\mathcal{T}, \cdot) is a group.

To motivate definition (A.1), let us consider two plane waves $E_l(x) = A \exp(ik(x)) + B \exp(-ik(x))$, $x \leq 0$, and $E_r(x) = C \exp(ik(x-L)) + D \exp(-ik(x-L))$, $x \geq L$, left and right of a dielectric with a homogeneous refractive index n . Hence their amplitudes are coupled as

$$\begin{pmatrix} C \\ D \end{pmatrix} = S_{n,1} \cdot P_{nL} \cdot S_{1,n} \begin{pmatrix} A \\ B \end{pmatrix}. \quad (\text{A.3})$$

where S_{n_1, n_2} couples the amplitudes at the intersection from a region with refractive index n_1 to a region with index n_2 and P_d denotes the propagation matrix over a distance d , i. e.

$$S_{n_1, n_2} = \frac{1}{2n_2} \begin{pmatrix} n_2 + n_1 & n_2 - n_1 \\ n_2 - n_1 & n_2 + n_1 \end{pmatrix} \quad \text{and} \quad P_d = \begin{pmatrix} e^{ikd} & 0 \\ 0 & e^{-ikd} \end{pmatrix}. \quad (\text{A.4})$$

One can easily show that $S_{n,1} \cdot P_{nL} \cdot S_{1,n} = T(r_h, r_h, t_h)$, with r_h and t_h as given in (24). But the attempt to construct a total transfer matrix for stacked media such as $S_{n_K,1} \cdot P_{n_K d_K} \cdot S_{n_{K-1}, n_K} \cdots S_{n_2, n_1} \cdot P_{n_1 d_1} \cdot S_{1, n_1}$ with arbitrary $n_i, d_i, i = 1, \dots, K$, will show that one reflection coefficient is not enough. However, such a system can be described by a more general $T(r_1, r_2, t) \in \mathcal{T}$ such that $B = r_1 A + tD$ and $C = r_2 D + tA$.

Appendix B. Analytical approximations for electric fields and forces for small deformations

In section 2 and in an earlier work [11] we showed that for equally spaced slices the amplitudes of the electric fields are related as $(A_{j+1}, B_{j+1})^T = T_h^j (A_1, B_1)^T$, with $T_h := P_{d_0} M_{\text{BS}}$. Choosing the coupling ζ as in (6), the eigenvalues of T_h read $\exp(\pm inkd_0)$. This leads to

$$\lim_{N \rightarrow \infty} T_h^{j-1} =: T(x) = \frac{1}{2n} \begin{pmatrix} f(-x) + g(-x) & f(x) - g(x) \\ f(-x) - g(-x) & f(x) + g(x) \end{pmatrix} \quad (\text{B.1})$$

where $x = \lim_{N \rightarrow \infty} L(j-1)/(N-1)$ and

$$\begin{aligned} f(x) &= n \cos(nkx) - i \sin(nkx), \\ g(x) &= n \cos(nkx) - in^2 \sin(nkx). \end{aligned} \quad (\text{B.2})$$

Allowing small local density variations $\tilde{d}_j - d_0 = \Delta_j$ we may use $P_{d_j} \simeq P_{d_0} + ik\Delta_j \sigma_z P_{d_0}$ to expand the relation between the field amplitudes from (4) as

$$\begin{pmatrix} A_{j+1} \\ B_{j+1} \end{pmatrix} \simeq \left[T_h^j + ik \sum_{m=1}^j \Delta_m T_h^{j-m} \sigma_z T_h^m \right] \begin{pmatrix} A_1 \\ B_1 \end{pmatrix}, \quad (\text{B.3})$$

where $\sigma_z = \text{diag}(1, -1)$. In the limit of infinitely many slices within a finite length L , the sum above can be rewritten to an integral and we obtain

$$\begin{pmatrix} A(x) \\ B(x) \end{pmatrix} \simeq \left[T(x) + ik \int_0^x u'(y) T(x-y) \sigma_z T(y) dy \right] \begin{pmatrix} A(0) \\ B(0) \end{pmatrix}. \quad (\text{B.4})$$

Since $\lim_{N \rightarrow \infty} M_{\text{BS}} = \text{id}_2$, the total reflection and transmission coefficients for the displaced object can be read off and expanded in linear order of u' from equations (5) and (B.4)

$$\begin{aligned} t &\simeq t_h + \frac{2ik}{(f(L)+g(L))^2} \int_0^L u'(y) (f(y)f(L-y) + g(y)g(L-y)) dy, \\ r_l &\simeq r_h + \frac{2ik}{(f(L)+g(L))^2} \int_0^L u'(y) (f(L-y)^2 - g(L-y)^2) dy, \\ r_r &\simeq r_h + \frac{2ik}{(f(L)+g(L))^2} \int_0^L u'(y) (f(y)^2 - g(y)^2) dy. \end{aligned} \quad (\text{B.5})$$

Here r_h and t_h denote the reflection and transmission amplitudes of a homogeneous medium with length L and refractive index n , as given in (24). As mentioned in section 2.1 we find that symmetric local strain, i.e. $u'(x) = u'(L-x)$, $x \in [0, L]$, results in $r_l \simeq r_r$ and antisymmetric strain gives $t \simeq t_h$ and $r_l - r_h \simeq r_h - r_r$.

Using the reflection and transmission amplitudes from (B.5) to replace $B(0) = r_l A(0) + t D(L)$ in (B.4) leads to analytical approximations for the local field amplitudes inside a deformed medium

$$\begin{aligned} A(x) &\simeq a_h(x) + \int_0^x u'(y) a_x(x, y) dy + \int_0^L u'(y) a_L(x, y) dy, \\ B(x) &\simeq b_h(x) + \int_0^x u'(y) b_x(x, y) dy + \int_0^L u'(y) b_L(x, y) dy, \end{aligned} \quad (\text{B.6})$$

with the individual terms reading

$$\begin{aligned} a_h(x) &= \frac{A_0(f(L-x) + g(L-x)) + D_L(f(x) - g(x))}{f(L) + g(L)}, \\ b_h(x) &= \frac{A_0(f(L-x) - g(L-x)) + D_L(f(x) + g(x))}{f(L) + g(L)}, \\ a_x(x, y) &= \frac{ik}{n(f(L) + g(L))} \left(A_0(f(L-y)f(y-x) + g(L-y)g(y-x)) + \right. \\ &\quad \left. + D_L(f(y)f(y-x) - g(y)g(y-x)) \right), \\ b_x(x, y) &= \frac{-ik}{n(f(L) + g(L))} \left(A_0(f(L-y)f(x-y) - g(L-y)g(x-y)) + \right. \\ &\quad \left. + D_L(f(y)f(x-y) + g(y)g(x-y)) \right), \\ a_L(x, y) &= \frac{ik(f(x) - g(x))}{n(f(L) + g(L))^2} \left(A_0(f(L-y)^2 - g(L-y)^2) + \right. \\ &\quad \left. + D_L(f(y)f(L-y) + g(y)g(L-y)) \right), \\ b_L(x, y) &= \frac{ik(f(x) + g(x))}{n(f(L) + g(L))^2} \left(A_0(f(L-y)^2 - g(L-y)^2) + \right. \\ &\quad \left. + D_L(f(y)f(L-y) + g(y)g(L-y)) \right). \end{aligned} \quad (\text{B.7})$$

The functions f and g are given in (B.2), the amplitudes at the boundary $A_0 \equiv A(0)$ and $D_L \equiv D(L)$ are determined by the incoming intensities and the displacement and can be read off from (22).

To obtain an approximation for the forces we use (28), take the limit $\mathcal{F}(x) := \lim_{N \rightarrow \infty} N F_j / L$ with $\lim_{N \rightarrow \infty} N \zeta / L = k(n^2 - 1)/2$ and insert the amplitudes from (B.6) to find

$$\begin{aligned} \mathcal{F}(x) &= \frac{k\varepsilon_0}{2} \text{Im} \{ (n^2 - 1) (A(x) + B(x))(A(x) - B(x))^* \} \\ \mathcal{F}(x) &\simeq \mathcal{F}_h(x) + \int_0^x u'(y) \mathcal{F}_x(x, y) dy + \int_0^L u'(y) \mathcal{F}_L(x, y) dy, \end{aligned} \quad (\text{B.8})$$

where

$$\begin{aligned}
\mathcal{F}_h(x) &= \frac{2k\varepsilon_0}{|(f(L)+g(L))|^2} \text{Im}\{(n^2 - 1)(A_0 f(L - x) + D_L f(x))(A_0 g(L - x) - D_L g(x))^*\} \\
\mathcal{F}_x(x) &= \frac{k\varepsilon_0}{2} \text{Im}\left\{(n^2 - 1) \left[(a_h(x) - b_h(x))^*(a_x(x, y) + b_x(x, y)) + \right. \right. \\
&\quad \left. \left. (a_h(x) + b_h(x))(a_x(x, y) - b_x(x, y))^* \right] \right\} \\
\mathcal{F}_L(x) &= \frac{k\varepsilon_0}{2} \text{Im}\left\{(n^2 - 1) \left[(a_h(x) - b_h(x))^*(a_L(x, y) + b_L(x, y)) + \right. \right. \\
&\quad \left. \left. (a_h(x) + b_h(x))(a_L(x, y) - b_L(x, y))^* \right] \right\}
\end{aligned} \tag{B.9}$$

with the terms a_x and b_x as given above in (B.7).

Just like the field amplitudes in (B.6) and the reflection and transmission coefficients in (B.5), the above result is only an approximation for the case of small deformation u' . That is, we neglect products of $\Delta_l \Delta_m$ in (B.3) and hence also correlations of type $\int \int u'(y_1)u'(y_2) \dots dy_1 dy_2$. But a comparison of the approximated results in the continuous limit with solutions of the wave equation (20) or numerical computations for a large but finite number of beam splitters confirmed that this first order expansion is sufficient for the scope of parameters used in this work.

References

- [1] A. Ashkin. Acceleration and trapping of particles by radiation pressure. *Physical Review Letters*, 24(4):156, January 1970.
- [2] T. W. Hänsch and A. L. Schawlow. Cooling of gases by laser radiation. *Optics Communications*, 13(1):68–69, 1975.
- [3] W. D. Phillips. Laser cooling and trapping of neutral atoms. *Reviews of Modern Physics*, 70(3):721–742, 1998.
- [4] D. J. Stevenson, F. Gunn-Moore, and K. Dholakia. Light forces the pace: optical manipulation for biophotonics. *Journal of biomedical optics*, 15:041503, 2010.
- [5] M. Padgett and R. Di Leonardo. Holographic optical tweezers and their relevance to lab on chip devices. *Lab on a chip*, 11(7):1196–1205, 2011.
- [6] G. Thalhammer, R. Steiger, S. Bernet, and M. Ritsch-Marte. Optical macro-tweezers: trapping of highly motile micro-organisms. *Journal of Optics*, 13:044024, 2011.
- [7] T. J. Kippenberg and K. J. Vahala. Cavity optomechanics: Back-Action at the mesoscale. *Science*, 321(5893):1172–1176, August 2008.
- [8] G.S. Wiederhecker, L. Chen, A. Gondarenko, and M. Lipson. Controlling photonic structures using optical forces. *Nature*, 462(7273):633–636, 2009.
- [9] M. Mansuripur. Radiation pressure and the linear momentum of the electromagnetic field. *Optics Express*, 12(22):5375–5401, November 2004.
- [10] A. Zakharian, M. Mansuripur, and J. Moloney. Radiation pressure and the distribution of electromagnetic force in dielectric media. *Optics Express*, 13(7):2321–2336, April 2005.
- [11] M. Sonnleitner, M. Ritsch-Marte, and H. Ritsch. Optical forces, trapping and strain on extended dielectric objects. *EPL (Europhysics Letters)*, 94(3):34005, May 2011.
- [12] I. H. Deutsch, R. J. C. Spreeuw, S. L. Rolston, and W. D. Phillips. Photonic band gaps in optical lattices. *Physical Review A*, 52(2):1394–1410, 1995.
- [13] J. Asbóth, H. Ritsch, and P. Domokos. Optomechanical coupling in a one-dimensional optical lattice. *Physical Review A*, 77(6), 2008.
- [14] L. D. Landau and E. M. Litschitz. *Theory of Elasticity*, volume 7 of *Course on Theoretical Physics*. Pergamon Press, third edition, 1986.

- [15] B. Lautrup. *Physics of Continuous Matter*. IoP Publishing, 2005.
- [16] M. Born and E. Wolf. *Principles of Optics, Electromagnetic Theory of Propagation, Interference and Diffraction of Light*. Pergamon Press, Oxford, sixth edition, 1993.
- [17] J. D. Jackson. *Classical Electrodynamics*. Wiley, New York, third edition, 1999.
- [18] A. Xuereb, P. Domokos, J. Asbóth, P. Horak, and T. Freearge. Scattering theory of cooling and heating in optomechanical systems. *Physical Review A*, 79(5):53810, 2009.
- [19] C. Cohen-Tannoudji. Atomic motion in laser light. In J. Dalibard, J.-M. Raimond, and J. Zinn-Justin, editors, *Fundamental Systems in Quantum Optics, Proceedings of the Les Houches Summer School, Session LIII*, pages 1–164. Elsevier Science Publishers, 1992.
- [20] P. Zemánek, A. Jonáš, P. Ják, J. Ježek, M. Šerý, and M. Liška. Theoretical comparison of optical traps created by standing wave and single beam. *Optics Communications*, 220(4-6):401–412, 2003.
- [21] T. Čížmár, M. Šiler, M. Scaronerý, P. Zemánek, V. Garcés-Chávez, and K. Dholakia. Optical sorting and detection of submicrometer objects in a motional standing wave. *Physical Review B*, 74(3):035105, July 2006.
- [22] A. B. Stilgoe, T. A. Nieminen, G. Knöener, N. R. Heckenberg, and H. Rubinsztein-Dunlop. The effect of mie resonances on trapping in optical tweezers. *Optics Express*, 16(19):15039–15051, 2008.
- [23] J. Guck, R. Ananthakrishnan, H. Mahmood, T. J. Moon, C. Casey Cunningham, and J. Käs. The optical stretcher: A novel laser tool to micromanipulate cells. *Biophysical Journal*, 81(2):767–784, 2001.
- [24] S. Rancourt-Grenier, M. T. Wei, J. J. Bai, A. Chiou, P. P. Bareil, P. L. Duval, and Y. Sheng. Dynamic deformation of red blood cell in dual-trap optical tweezers. *Optics Express*, 18(10):10462–10472, 2010.
- [25] A. Ashkin and J. M. Dziedzic. Radiation pressure on a free liquid surface. *Physical Review Letters*, 30(4):139–142, 1973.
- [26] A. Casner and J. P. Delville. Giant deformations of a liquid-liquid interface induced by the optical radiation pressure. *Physical review letters*, 87(5):54503, 2001.
- [27] R. N. C. Pfeifer, T. A. Nieminen, N. R. Heckenberg, and H. Rubinsztein-Dunlop. Colloquium: Momentum of an electromagnetic wave in dielectric media. *Reviews of Modern Physics*, 79(4):1197, 2007.
- [28] S. M. Barnett and R. Loudon. The enigma of optical momentum in a medium. *Philosophical Transactions of the Royal Society A: Mathematical, Physical and Engineering Sciences*, 368(1914):927–939, 2010.